Cooperative Synchronization and Channel Estimation in Wireless Sensor Networks

Mi-Kyung Oh, Xiaoli Ma, Georgios B. Giannakis, and Dong-Jo Park

Abstract: **A critical issue in applications involving networks of wireless sensors is their ability to synchronize, and mitigate the fading propagation channel effects. Especially when distributed "slave" sensors (nodes) reach-back to communicate with the "master" sensor (gateway), low power cooperative schemes are well motivated. Viewing each node as an antenna element in a multi-input multi-output (MIMO) multi-antenna system, we design pilot patterns to estimate the multiple carrier frequency offsets (CFO), and the multiple channels corresponding to each node-gateway link. Our novel pilot scheme consists of non-zero pilot symbols along with zeros, which separate nodes in a time division multiple access (TDMA) fashion, and lead to low complexity schemes because CFO and channel estimators per node are decoupled. The resulting training algorithm is not only suitable for wireless sensor networks, but also for synchronization and channel estimation of single- and multi-carrier MIMO systems. We investigate the performance of our estimators analytically, and with simulations.**

Index Terms: **Channel estimation, Cramér-Rao bound, multi-input multi-output (MIMO), sensor networks, synchronization.**

I. INTRODUCTION

There has been a growing interest towards wireless sensor networks that emerge as a new wireless network paradigm capitalizing on the cooperation among a large number of sensors [1]. A distinct feature of such networks is that reliability and fault tolerance is achieved through combining information from distributed sensors. These characteristics are attractive for both commercial and military communication networks [1]–[2]. Moreover, efforts are under way to standardize the various layers of wireless sensor network communications; the IEEE 802.15.4 low rate wireless personal area network (WPAN) standard, and IEEE 1451.5 wireless smart transducer interface standard [3].

A bulk of research in wireless sensor networks focuses on low power cooperative schemes. However, most works assume error-free communication channels, and perfect synchronization between each node-gate link [4]. Since pragmatic wireless links entail channel-induced interference, as well as timing and frequency offsets, it is necessary to account for these effects when designing distributed sensor networks. This motivates us to pur-

M.-K. Oh and D.-J. Park are with the Department of Electrical and Computer Science, Korea Advanced Institute of Science and Technology (KAIST), 373-1, Guseong-dong, Yuseong-gu, Daejon, 305-701, Republic of Korea, email: jeniper@armi.kaist.ac.kr, djpark@ee.kaist.ac.kr.

X. Ma is with the Department of Electrical and Computer Engineering, Auburn University, Auburn, AL 36849, U.S.A., email: xiaoli@eng.auburn.edu.

G. B. Giannakis is with the Department of Electrical and Computer Engineering, University of Minnesota, 200 Union Street, Minneapolis, MN 55455, U.S.A., email: georgios@ece.umn.edu.

sue channel and carrier frequency offset (CFO) estimation algorithms for wireless sensor networks.

We suppose that each sensor node has a single antenna to transmit and receive data, while the central processing unit (a.k.a. gateway, or fusion center) is capable of deploying several receive antennas. In this setting, the overall sensor network can be viewed as multi-antenna point to point link. The ergodic (average) capacity of wireless multi-antenna channels can increase linearly with the number of antennas at the transmitter/receiver, provided that perfect channel estimates are available at the receiver [5]–[7]. Errors in the channel and synchronization estimates can significantly degrade error performance, and capacity. On the other hand, as the number of sensor nodes increases, channel estimation becomes more challenging because the number of unknowns increases accordingly.

Since this multi-sensor environment is similar to a multi-antenna system, existing multi-input multi-output (MIMO) channel estimators apply. For example, the channel estimators in [8]–[10] can be recast in a wireless sensor network setting, even though they do not address CFO estimation. The importance of the latter can be appreciated if we recall that sensor oscillators can never be perfectly synchronous. Furthermore, even with ideal oscillators CFOs are present in a mobile environment with pronounced Doppler shifts. For point to point links, existing CFO estimators can be either data-aided [11], [12], or non-data aided [13]. Blind methods typically require longer data records, and have rather high computational complexity. On the other hand, data-aided schemes based on training symbols (known to both transmitter and receiver) are bandwidth consuming, but they are computationally attractive. Since sensors are generally limited in power and computational capabilities, training schemes with low complexity and low duty cycle are well motivated.

In this paper, we consider cooperative synchronization and channel estimation in wireless sensor networks. Specifically, we design training patterns for estimating the associated multiple CFOs and frequency selective channels. Our goal should be contrasted with previous works that either estimate a single CFO common to all transmit antennas [14], or a single-input single-output (SISO) channel [12]. We design training symbols that enable decoupling CFO and channel estimation from sensor to sensor, based on time division multiple access (TDMA), which in turn leads to low complexity and low duty cycle operations. Unlike existing algorithms [11], [12], our CFO estimators have full acquisition range, and the proposed channel estimators are not only suitable for wireless sensor networks, but also apply to single carrier multi-antenna point to point links. In addition, our training scheme can be directly applied to a multi-user multi-carrier system having distinct CFO between
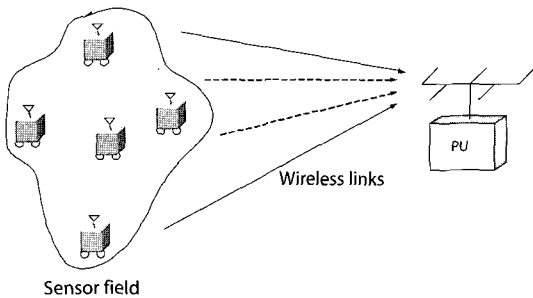
Fig. 1. Schematic system model for wireless sensor networks.

each transmit-receive link, which has not been considered in any existing literatures.

The rest of the paper is organized as follows. In Section II, we describe our system model. The algorithms for estimating multiple CFOs and channels are derived in Section III. In Section IV, we show that our estimator can be used for multi-user multi-carrier systems. Performance of our estimators is analyzed in Section V. In Section VI, simulation results demonstrate the potential of our algorithms, while Section VII concludes this paper.

Notation: Upper (lower) bold face letters indicate matrices (column vectors). Superscript $(\cdot)^{\mathcal{H}}$ will denote Hermitian, $(\cdot)^T$ transpose, and $(\cdot)^*$ conjugate. The real and imaginary parts are denoted as $\Re[\cdot]$ and $\Im[\cdot]$. $E[\cdot]$ and Var$[\cdot]$ will stand for expectation and variance, tr$[\cdot]$ for trace operation, and diag$[x]$ for a diagonal matrix with x on its main diagonal. For a vector, $\|\cdot\|$ denotes the Euclidean norm. We will use $[\mathbf{A}]_{k,m}$ to denote the (k,m)-th entry of a matrix $\mathbf{A}$, and $[x]_m$ for the m-th entry of the column vector x; $\mathbf{I}_N$ to denote the $N \times N$ identity matrix; $[\mathbf{F}_N]_{m,n} = N^{(1/2)}\exp(-j2\pi mn/N)$ the $N \times N$ fast fourier transform (FFT) matrix.

II. SYSTEM MODEL AND ASSUMPTIONS

Fig. 1 depicts our system model that includes N_s sensors (nodes) in the sensor field communicating with a central processing unit (PU) equipped with multiple antennas signalling over wireless channels. The fading channels between each sensor and the PU entail rich scattering and have delay spread greater than the symbol period, i.e., they are frequency selective. Define the discrete-time baseband equivalent channel from the μ-th sensor to the ν-th receive antenna as $h^{(\nu,\mu)}(l)$, $l \in [0,L]$. We note that the channel sounder can be used to characterize the wireless channel [15]. In addition to multi-path, this equivalent channel incorporates also transmit- and receive filters, as well as timing offsets in the form of pure delay factors. Let the CFO between oscillator of the μ-th sensor and the ν-th receive antenna of the PU be denoted as $f_o^{(\nu,\mu)}$ (in Hz), which could be due to Doppler, or, mismatch between sensor-receive oscillators.

To estimate the N_s channels and the N_s CFOs for each receive antenna, pilot symbols $\{p_\mu(n)\}_{\mu=1}^{N_s}$, $n \in \mathcal{I} := [0, N-1]$, are transmitted by the μ-th sensor. Samples at the ν-th antenna output of the PU can be written as

$$x_\nu(n) = \sum_{\mu=1}^{N_s} e^{j\omega_o^{(\nu,\mu)}n} \sum_{l=0}^{L} h^{(\nu,\mu)}(l)p_\mu(n-l) + \eta_\nu(n) \quad (1)$$

where $n \in [0, N-1]$; $\omega_o^{(\nu,\mu)} := 2\pi f_o^{(\nu,\mu)}T$ is the normalized CFO with T denoting sampling period which is chosen equal to the symbol period; and $\eta_\nu(n)$ is zero-mean, white, complex Gaussian distributed noise with variance $\sigma_{\eta_\nu}^2$.

The PU is responsible for scheduling sensor transmissions. To facilitate scheduling, we require that the sensor signals be delivered to the PU with a small delay, which can be ensured if the PU transmits a beacon, that sensors can synchronize to. As timing acquisition is beyond the scope of this paper, we suppose that it has been accomplished, and incorporate residual timing errors in the channel order L. The information-bearing symbols are transmitted following the training preamble. Because the channel is frequency selective, time-dispersive interference emerges between information and training symbols. The received samples $x_\nu(n)$ in (1) correspond solely to the transmitted pilots, excluding those that contain interference from the information symbols.

On the other hand, sensor networks need to handle thousands of sensor nodes. We assume that this problem can be solved by adapting a very efficient medium access control (MAC) techniques to accommodate thousands of sensor nodes [3], which is beyond the scope of this paper. In this paper, we consider multiple access in the physical layer, for which limited number of sensor nodes can access the channel at the same time.

III. ESTIMATING MULTIPLE CFOS AND CHANNELS

We wish to estimate the carrier frequency offsets $\{\omega_o^{(\nu,\mu)}\}_{\mu=1}^{N_s}$ and the channels $\{\mathbf{h}^{(\nu,\mu)}\}_{\mu=1}^{N_s}$, where $\mathbf{h}^{(\nu,\mu)} := [h^{(\nu,\mu)}(0), \cdots, h^{(\nu,\mu)}(L)]^T$, based on the ν-th antenna received samples $\{x_\nu(n)\}_{n=0}^{N-1}$ and the pilots $\{p_\mu(n)\}_{\mu=1}^{N_s}$, $n \in \mathcal{I}$. Equation (1) shows that estimating CFOs and channels from $x_\nu(n)$ and $p_\mu(n)$ is a non-linear problem, whose solution is computationally prohibitive. We will thus decouple CFO and channel estimation for each sensor using a TDMA scheme, and we will show that the resulting estimators enjoy low complexity and guarantee identifiability. TDMA is chosen because it leads to the desirable low duty cycle sensor operation, which is important for energy efficiency.

For clarity, we will start our design of pilot symbols with a single sensor. Design of pilot symbols for multiple sensors will be described in Section III-B.

A. Single Sensor

For a single sensor, we drop the sensor index μ, and thus (1) reduces to

$$x_\nu(n) = e^{j\omega_o^{(\nu)}n} \sum_{l=0}^{L} h^{(\nu)}(l)p(n-l) + \eta_\nu(n) \quad (2)$$

where $n \in [0, N-1]$, and N is the total number of pilot symbols. Let us define the set of pilot symbols as $\mathcal{I}_p := [0, N_p-1]$, where $N_p = N - L$.

To further reduce complexity, we also wish to separate CFO from channel estimation. Note that the CFO appears as a multiplicative factor in each received symbol. This suggests selecting pilots to keep the sum in (2) identical for at least two $x_\nu(n)$'s, and estimating the CFO from their phase difference.

Targeting such an approach, we select pilot symbols as follows.

$$p(n) = \begin{cases} \sqrt{\mathcal{E}_p}\rho^n & , \; n \in \mathcal{I}_p \\ 0 & , \; n \in \mathcal{I}_{p,o} \end{cases} \tag{3}$$

where ρ is an arbitrary complex number with $|\rho|^2 = 1$, and $\mathcal{E}_p$ is the energy of the training symbol, which could be chosen equal to the energy of the information symbol $\mathcal{E}_s$. The set of zero pilots is defined as $\mathcal{I}_{p,o} := [N_p, N - 1]$.

Substituting (3) into (2), we obtain

$$x_\nu(n) = \sqrt{\mathcal{E}_p} e^{j\omega_o^{(\nu)} n} \rho^n \sum_{l=0}^{L} h^{(\nu)}(l)\rho^{-l} + \eta_\nu(n) \tag{4}$$

for $n \in [L, N_p - 1]$. If $H^{(\nu)}(\rho) := \sum_{l=0}^{L} h^{(\nu)}(l)\rho^{-l} \neq 0$, the noise free version of (4) can be written as

$$x_\nu(n + 1) = \rho e^{j\omega_o^{(\nu)}} x_\nu(n), \; \text{for } n \in [L, N_p - 2]. \tag{5}$$

Clearly, we require $N_p - 2 \geq L$ in (5), which implies that the minimum number of pilots is $N_p \geq L + 2$. The CFO estimator follows easily from (5) in closed-form

$$\hat{\omega}_o^{(\nu)} = \tan^{-1}\left\{ \left(\sum_{n=L}^{N_p-2} \Im[x_\nu(n+1)\rho^* x_\nu^*(n)] \right) \Big/ \left(\sum_{n=L}^{N_p-2} \Re[x_\nu(n+1)\rho^* x_\nu^*(n)] \right) \right\} \tag{6}$$

and should be intuitively expected since in the absence of noise, the phase of $x_\nu(n + 1)\rho^* x_\nu^*(n)$ equals $\omega_o^{(\nu)}$. We also note from (6) that the accuracy of CFO estimator increases, as the number of training symbols N_p increases.

Based on the estimated CFO in (6), we can compensate for the CFO $\omega_o^{(\nu)}$ from $x_\nu(n)$ in (2), and proceed with channel estimation. To derive our channel estimator, we temporarily assume that the CFO estimate is perfect, i.e., $\hat{\omega}_o^{(\nu)} = \omega_o^{(\nu)}$. By simply forming $y_\nu(n) := \exp(-j\hat{\omega}_o^{(\nu)} n)x_\nu(n)$, we then obtain

$$y_\nu(n) = \sum_{l=0}^{L} h^{(\nu)}(l)p(n - l) + \eta(n), \; \text{for } n \in [0, N - 1]. \tag{7}$$

Using the least-squares (LS) approach, we can easily estimate the channel as (c.f., (7))

$$\hat{\mathbf{h}}_{LS}^{(\nu)} = (\mathbf{P}^{\mathcal{H}}\mathbf{P})^{-1}\mathbf{P}^{\mathcal{H}}\mathbf{y}_\nu \tag{8}$$

where $\mathbf{P}$ is a Toeplitz matrix with entries $[\mathbf{P}]_{i,j} := p(i-j)$, $0 \leq i \leq N-1$, $0 \leq j \leq L$, and $\mathbf{y}_\nu := [y_\nu(0), \cdots, y_\nu(N-1)]^T$. If the channel covariance matrix $\mathbf{R}_{h^{(\nu)}} := E[\mathbf{h}^{(\nu)}\mathbf{h}^{(\nu)\mathcal{H}}]$ and the noise variance σ_η^2 are available, a linear minimum mean square error (LMMSE) channel estimator can be used instead of the LS one in (8), which can be expressed as

$$\hat{\mathbf{h}}_{LMMSE}^{(\nu)} = (\sigma_\eta^2 \mathbf{R}_{h^{(\nu)}}^{-1} + \mathbf{P}^{\mathcal{H}}\mathbf{P})^{-1}\mathbf{P}^{\mathcal{H}}\mathbf{y}_\nu. \tag{9}$$

The natural question that arises at this point is whether we can always find ρ such that $H^{(\nu)}(\rho) \neq 0$. If ρ in (3) satisfies

$H^{(\nu)}(\rho) = 0$, then CFO is non-identifiable. To guarantee identifiability, one needs to collect additional observations (4) for more than L distinct ρ's. If we choose $(L + 1)$ points $\rho_l \in C$, $l = 0, \cdots, L$, such that $\rho_m \neq \rho_n, \forall m \neq n$, we have

$$\begin{pmatrix} H^{(\nu)}(\rho_0) \\ H^{(\nu)}(\rho_1) \\ \vdots \\ H^{(\nu)}(\rho_L) \end{pmatrix} = \begin{pmatrix} 1 & \rho_0^{-1} & \cdots & \rho_0^{-L} \\ 1 & \rho_1^{-1} & \cdots & \rho_1^{-L} \\ \vdots & \vdots & \ddots & \vdots \\ 1 & \rho_L^{-1} & \cdots & \rho_L^{-L} \end{pmatrix} \begin{pmatrix} h^{(\nu)}(0) \\ h^{(\nu)}(1) \\ \vdots \\ h^{(\nu)}(L) \end{pmatrix}$$

$$:= \mathbf{\Theta}\mathbf{h}^{(\nu)}. \tag{10}$$

We note that the Vandermonde matrix $\mathbf{\Theta}$ in (10) has always full rank, since $\mathbf{h}^{(\nu)} \neq \mathbf{0}$, and we can obtain at least one nonzero $H^{(\nu)}(\rho_l)$ among $(L + 1)$ blocks. The set $\{\rho_l\}_{l=0}^{L}$ is clearly not unique. For example, if we select $\rho_l = e^{j2\pi l/(L+1)}$ for $l = 0, 1, \cdots, L$, then $\mathbf{\Theta}$ in (10) becomes unitary matrix $\sqrt{(L+1)}\mathbf{F}_{L+1}$, where $\mathbf{F}_{L+1}$ is an $(L + 1) \times (L + 1)$ FFT matrix.

B. Multiple Sensors

In the previous subsection, we designed the pilot pattern to estimate the CFO and channel corresponding to a single sensor. We found from (3) that at least $L + 2$ consecutive nonzero pilot symbols guarded by L zeros are sufficient. In this subsection, we consider multiple sensors, where distinct pairs of sensors and receive antenna elements have distinct channels and CFOs, i.e., there are N_s channels, and N_s CFOs to be estimated per receive antenna. In the following, we will show how relying on TDMA, we can design $\{p_\mu(n)\}_{\mu=1}^{N_s}$, $n \in \mathcal{I}$ for the μ-th sensor, so that signals from different sensors can be orthogonally separated at the PU. Let us recall from (1) that $\mathcal{I}$ was defined as the set of indices $n \in [0, N - 1] := \mathcal{I}$.

To estimate $\{\omega_o^{(\nu,\mu)}, \mathbf{h}^{(\nu,\mu)}\}_{\mu=1}^{N_s}$ on a per sensor basis, $\mathcal{I}$ should be orthogonally separated into N_s non-overlapping subsets, i.e., $\{\mathcal{I}_p^\mu\}_{\mu=1}^{N_s}$ should obey $\mathcal{I}_p^{\mu_1} \cap \mathcal{I}_p^{\mu_2} = \emptyset$, $\forall \mu_1 \neq \mu_2$.

If a sequence of length N_p is linearly convolved with a channel of length $L + 1$, the resulting sequence has length $N_p + L$. This means that L guard zeros should be appended to N_p consecutive non-zero pilots to avoid interference among sensors. Thus, time is divided in sensor-specific slots, with each slot containing $N_p + L$ symbol periods. This implies that the whole training block per sensor should have length $N = N_s(N_p + L)$. Now we can divide the $N_p + L$ slots per sensor into two sets

$$\mathcal{I}_p^\mu := [(N_p + L)(\mu - 1), (N_p + L)(\mu - 1) + N_p - 1],$$

$$\mathcal{I}_{p,o}^\mu := [(N_p + L)(\mu - 1) + N_p, (N_p + L)\mu - 1]$$

where $\mathcal{I}_p^\mu \cap \mathcal{I}_{p,o}^\mu = \emptyset, \forall \mu$, and the sets $\mathcal{I}_p^\mu$ and $\mathcal{I}_{p,o}^\mu$ represent the parts of N_p nonzero pilot symbols and L guard zeros corresponding to the μ-th sensor.

Similar to (3), our pilot pattern can be chosen as

$$p_\mu(n) = \begin{cases} \sqrt{\mathcal{E}_p}\rho^n & , \; n \in \mathcal{I}_p^\mu \\ 0 & , \; \text{otherwise} \end{cases}. \tag{11}$$

The data in (1) can now be orthogonally separated into N_s sets of observations, each having the same structure as that for a sin-

gle sensor. For the μ-th sensor, we thus have

$$
\begin{aligned}
x_{\nu,\mu}(n) &= e^{j\omega_o^{(\nu,\mu)}n} \sum_{l=0}^{L} h^{(\nu,\mu)}(l)p_\mu(n-l) + \eta_\nu(n) \\
&= \sqrt{\mathcal{E}_p}e^{j\omega_o^{(\nu,\mu)}n}\rho^n \sum_{l=0}^{L} h^{(\nu,\mu)}(l)\rho^{-l} + \eta_\nu(n)
\end{aligned}
\tag{12}
$$

where $n \in [(N_p+L)(\mu-1), (N_p+L)\mu - 1]$.

By using the fact that $x_{\nu,\mu}(n+1) = \rho e^{j\omega_o^{(\nu,\mu)}}x_{\nu,\mu}(n)$ in (12), we can estimate $\hat{\omega}_o^{(\nu,\mu)}$ and $\hat{h}^{(\nu,\mu)}$ for the μ-th sensor in the ν-th antenna of the PU using (6) and (8) as follows.

$$
\begin{aligned}
\hat{\omega}_o^{(\nu,\mu)} = \\
\tan^{-1}\Bigg\{ &\left(\sum_{n=(N_p+L)(\mu-1)+L}^{(N_p+L)(\mu-1)+N_p-2} \Im[x_{\nu,\mu}(n+1)\rho^*x_{\nu,\mu}^*(n)]\right) \\
/ &\left(\sum_{n=(N_p+L)(\mu-1)+L}^{(N_p+L)(\mu-1)+N_p-2} \Re[x_{\nu,\mu}(n+1)\rho^*x_{\nu,\mu}^*(n)]\right) \Bigg\}
\end{aligned}
\tag{13}
$$

and

$$
\hat{h}_{LS}^{(\nu,\mu)} = (\mathbf{P}^{\mathcal{H}}\mathbf{P})^{-1}\mathbf{P}^{\mathcal{H}}\mathbf{y}_{\nu,\mu}
\tag{14}
$$

where $\mathbf{y}_{\nu,\mu} := [y_{\nu,\mu}((N_p+L)(\mu-1)), \cdots, y_{\nu,\mu}((N_p+L)\mu-1)]^T$ with entry $y_{\nu,\mu}(n) = \exp(-j\hat{\omega}_o^{(\nu,\mu)}n)x_{\nu,\mu}(n)$, and $\mathbf{P}$ has the same structure as that of (8). Notice that we utilize maximally the advantages of TDMA scheduling to estimate CFOs and channels.

C. Further Considerations

We have proposed CFO and channel estimators for wireless sensor networks. Following remarks are pertinent to our CFO and channel estimators in (6) and (8).

1. The training patten for a single sensor consists of N_p consecutive non-zero pilots, and L guard zeros. To guarantee identifiability for any channel and any CFO $\omega_o^{(\nu,\mu)} \in [-\pi, \pi)$, one needs to collect at least $(L+1)$ blocks for distinct ρ's.

2. Our CFO estimator in (6) is reminiscent of the one in [11], where [11] employed two consecutive and identical training blocks with block length N for the single antenna system. However, the acquisition range of our CFO estimator is $[-\pi, \pi)$ for any channel of order L, which is to be contrasted with [11] whose acquisition range is limited to $(1/N)[-\pi, \pi)$ and [17] whose acquisition range depends on the number of identical parts in a block. The performance comparison regarding this issue will be shown in Examples 1 and 4 of the Section VI.

3. The closed form estimator in (6) has lower complexity than the maximum likelihood estimator (MLE) in [12], which being nonlinear and statistical, requires many data blocks, and grid search.

4. For CFO and channel estimation, $L + 2$ non-zero pilots, equal to the number of unknowns ($L + 1$ channels and

Training							Payload	
N_p	L	N_p	L	N_p	L	L		
$\mathbf{p}_1$		0	0	0	0	0	0	Sensor 1
$\mathbf{p}_2$	0	0		0	0	0	0	Sensor 2
$\mathbf{p}_3$	0	0	0	0		0	0	Sensor 3

Fig. 2. Pilot pattern $\mathbf{p}_\mu$ with $N_s = 3$ sensors.

CFO), are only needed. This minimal training confirms band-width efficiency.

5. Our algorithm can be easily applied to packet transmissions, where the pilot part is attached to the payload part. The latter may be quite long, and L guard zeros are required to decouple it from the pilot part. In this case, CFO estimation using two identical packets required by [11] can not be used, since the resulting CFO acquisition range shrinks considerably.

6. There is a tradeoff between estimation accuracy and bandwidth efficiency. If more pilots are used, the performance of (6) can be improved, at the expense of bandwidth-efficiency, which will be demonstrated in Example 4 of the Section VI.

Additional remarks for the multi-sensor case are now in order.

1. The number of pilot slots per sensor is $N = (N_p + L)N_s$, where $N_p \geq L + 2$. The pilot pattern is depicted in Fig. 2, together with the payload part separated by L guard zeros. It follows by inspection that the training sequences of multiple sensors are scheduled in a TDMA fashion.

2. The duty cycle for the pilot part is just N_p/N, which implies that our scheme is energy efficient per sensor.

IV. APPLICATION TO MULTI-USER MULTI-CARRIER SYSTEMS

In the previous section, we proposed a training pattern for estimating multiple CFOs and multiple channels in wireless sensor networks where single-carrier transmissions were considered. Because orthogonal frequency division multiplexing (OFDM) has been widely adopted by many standards such as DAB, DVB, HyperLAN, IEEE 802.11a, and IEEE 802.16a, we want to apply our scheme to OFDM systems which exhibit sensitivity to CFO [23]. In this case, mobile users in an uplink orthogonal frequency division multiplex access (OFDMA) system are considered. In this section, we will show that the training pattern of the previous section can be also exploited to synchronize wireless MIMO systems that employ multi-carrier transmissions.

Considering multi-carrier operation, we suppose that the total number of subcarriers is $N := N_s(N_p + L)$, where N_p of them are used for data transmission, and L is the number of guard (virtual, or null) subcarriers per mobile user. Notice that N_s is the number of mobile users. The received samples at the ν-th antenna in the base station are given by

$$
\begin{aligned}
x_\nu(n) = & \sum_{\mu=1}^{N_s} e^{j\omega_o^{(\nu,\mu)}n} \sum_{l=0}^{L} h^{(\nu,\mu)}(l) \sum_{k=0}^{N-1} u_\mu(k)e^{j2\pi k(n-l)/N} \\
& + \eta_\nu(n), \quad n \in [0, N+L-1]
\end{aligned}
\tag{15}
$$

where the first L samples equal the last L ones and thus constitute the cyclic prefix (CP), and $u_\mu(k)$ is the pilot symbol transmitted on the k-th subcarrier of the μ-th mobile user. What is different in (15) relative to (1) is the transmission modality; i.e., N carriers are used here. We note that the other parameters in (15) are the same with those in (1) the same models of the channel and CFO. The vector-matrix counterpart of (15) after discarding the CP from (15) can be obtained as (see Appendix C).

$$\mathbf{y}_\nu = \sum_{\mu=1}^{N_s} e^{j\omega_o^{(\nu,\mu)}L} \mathbf{D}_N(\omega_o^{(\nu,\mu)}) \tilde{\mathbf{H}}^{(\nu,\mu)} \mathbf{F}_N^{\mathcal{H}} \mathbf{u}_\mu + \mathbf{v}_\nu \qquad (16)$$

where $\mathbf{y}_\nu := [y_\nu(0), \cdots, y_\nu(N-1)]^T$, and $\mathbf{u}_\mu := [u_\mu(0), \cdots, u_\mu(N-1)]^T$ should be judiciously designed to exploit the advantages of simple estimators in the previous section, $\tilde{\mathbf{H}}^{(\nu,\mu)}$ is a circulant matrix with first column $[h^{(\nu,\mu)}(0), \cdots, h^{(\nu,\mu)}(L), 0, \cdots, 0]^T$, and $\mathbf{F}_N$ is an N-point FFT matrix. The CFO matrix is defined as $\mathbf{D}_N(\omega_o^{(\nu,\mu)}) := \mathrm{diag}[1, e^{j\omega_o^{(\nu,\mu)}}, \cdots, e^{j\omega_o^{(\nu,\mu)}(N-1)}]$. We note that (16) is different from that in [16], where we derived CFO and channel estimators for MIMO-OFDM having common CFO between all transmit and receive antennas. In contrast, CFOs between each transmit-receive link are allowed to be distinct here.

To estimate $\{\omega_o^{(\nu,\mu)}\}_{\mu=1}^{N_s}$ and $\{\mathbf{h}^{(\nu,\mu)}\}_{\mu=1}^{N_s}$ in (16), we can use the cooperative synchronization scheme in the previous section, for which $\{\mathbf{u}_\mu\}_{\mu=1}^{N_s}$ should be cooperatively designed for each mobile user. To further study this application and the performance of our estimator, we introduce the vector-matrix counterpart of (1) as

$$\mathbf{x}_\nu = \sum_{\mu=1}^{N_s} \mathbf{D}_N(\omega_o^{(\nu,\mu)}) \mathbf{H}^{(\nu,\mu)} \mathbf{p}_\mu + \boldsymbol{\eta}_\nu \qquad (17)$$

where $\mathbf{H}^{(\nu,\mu)}$ is an $N \times N$ Toepliz matrix having the first column $[h^{(\nu,\mu)}(0), \cdots, h^{(\nu,\mu)}(L), 0, \cdots, 0]^T$, and $\mathbf{p}_\mu := [p_\mu(0), \cdots, p_\mu(N-1)]^T$. Recall that our focus on determining training symbols has been to find $\{\mathbf{p}_\mu\}_{\mu=1}^{N_s}$ so that estimators of CFO $\omega_o^{(\nu,\mu)}$ and channel $\mathbf{h}^{(\nu,\mu)}$ for each sensor can be orthogonally separated by TDMA.

If we select training symbols as $\mathbf{u}_\mu := \mathbf{F}_N \mathbf{p}_\mu$ in (16), where $\mathbf{p}_\mu$ follows the training pattern in (11), then (16) reduces to

$$\mathbf{x}_\nu = \sum_{\mu=1}^{N_s} e^{j\omega_o^{(\nu,\mu)}L} \mathbf{D}_N(\omega_o^{(\nu,\mu)}) \tilde{\mathbf{H}}^{(\nu,\mu)} \mathbf{p}_\mu + \boldsymbol{\eta}_\nu. \qquad (18)$$

We note that circulant and Toepliz matrices obey following property. $\tilde{\mathbf{H}}^{(\nu,\mu)} \mathbf{T}_{zp} = \mathbf{H}^{(\nu,\mu)} \mathbf{T}_{zp}$, where $\mathbf{T}_{zp} := [\mathbf{I}_{N-L} \; \mathbf{0}_{(N-L) \times L}]^T$. In our training scheme, the last L zeros in $\mathbf{p}_\mu$ allow $\tilde{\mathbf{H}}^{(\nu,\mu)}$ to be replaced by $\mathbf{H}^{(\nu,\mu)}$, which yields the same structure as in (17). Now we can directly use our estimators in (13) to estimate multiple CFOs $\{\omega_o^{(\nu,\mu)}\}_{\mu=1}^{N_s}$ and channels $\{\mathbf{h}^{(\nu,\mu)}\}_{\mu=1}^{N_s}$ from $\mathbf{x}_\nu$ in (18) for these multi-carrier systems.

V. PERFORMANCE ANALYSIS

To benchmark the performance of our estimators, we derive the Cramér-Rao lower bound (CRLB) of CFO. Because our CFO estimators among sensors are independent, the single-sensor CRLB is considered. Now the system model in (17) becomes $\mathbf{x} = \mathbf{D}_N(\omega_o)\mathbf{H}\mathbf{p} + \boldsymbol{\eta}$, where we drop the sensor indices (ν, μ). In this case, we can derive the CRLB as follows.

$$\mathrm{CRLB}_{\omega_o} = \left(\frac{1}{\sigma_\eta^2} \mathrm{tr} \left[\mathbf{D}(k) \mathbf{P} \mathbf{R}_h \mathbf{P}^{\mathcal{H}} \mathbf{D}(k) \right] \right)^{-1} \qquad (19)$$

where $\mathbf{D}(k) := \mathrm{diag}[0, 1, \cdots, N-1]$, $\mathbf{R}_h := E[\mathbf{h}\mathbf{h}^{\mathcal{H}}]$, and $\mathbf{P}$ is a Toeplitz matrix as in (8). We observe from (19) that as the number of training symbols N_p (and thus N) increases, the CRLB for CFO decreases.

For our estimator in (13), we consider the conditional mean and variance of $\hat{\omega}_o^{(\nu,\mu)}$ given $\omega_o^{(\nu,\mu)}$, and $\beta^{(\nu,\mu)}(n) := \sqrt{\mathcal{E}_p} \exp(j\omega_o^{(\nu,\mu)}n)\rho^n \sum_{l=0}^{L} h^{(\nu,\mu)}(l)\rho^{-l}$ for $n = (N_p+L)(\mu-1)+L, \cdots, (N_p+L)(\mu-1)+N_p-1$. For small errors, we can approximate the conditional mean and variance as follows.

$$E[\hat{\omega}_o^{(\nu,\mu)} - \omega_o^{(\nu,\mu)} | \omega_o^{(\nu,\mu)}, \{\beta_{\nu,\mu}(n)\}_{n=(N_p+L)(\mu-1)+L}^{(N_p+L)(\mu-1)+N_p-1}] = 0 \qquad (20)$$

and

$$\mathrm{Var}[\hat{\omega}_o^{(\nu,\mu)} | \omega_o^{(\nu,\mu)}, \{\beta_{\nu,\mu}(n)\}_{n=(N_p+L)(\mu-1)+L}^{(N_p+L)(\mu-1)+N_p-1}]$$
$$= \frac{1}{(N_p - L - 1)\mathrm{SNR}} \qquad (21)$$

where $\sigma_{\eta_\nu}^2 = N_o/2$, and $\mathrm{SNR} := (\mathcal{E}_p/\sigma_{\eta_\nu}^2) \sum_{l=0}^{L} |h^{(\nu,\mu)}(l)|^2$.

We note from (20) that the CFO estimator is conditionally unbiased for small errors, and from (21) the variance of the CFO estimator decreases as the number of training symbols and SNR increase.

VI. SIMULATIONS

We conducted simulations to verify the performance of our designs for wireless sensor networks. In all experiments, we considered an exponential channel model, for which taps are independent complex Gaussian random variables with average power profile that decays exponentially, and additive white Gaussian noise with zero-mean and variance $\sigma_{\eta_\nu}^2$. The information symbols were drawn from a QPSK constellation.

Example 1 (acquisition range of CFO estimator): To confirm the acquisition range of our CFO estimators, we compared against the single sensor $(N_s = 1)$ algorithm in [11] where the maximum likelihood estimator of the CFO was given based on two consecutive and identical training blocks. We note that our CFO estimation can be done within a block as shown in (3). Fig. 3 depicts "true CFO" versus "estimated CFO" when the channel order is $L = 3$ and the block length N is 8 and 12. The ideal line, for which the estimated CFO exactly follows the true CFO, is also shown for comparison. We deduce from Fig. 3 that our CFO estimator enjoys full acquisition range like ideal case, while the algorithm in [11] has the limited acquisition range, i.e., the CFO estimator of [11] fails to estimate CFO in the out of its acquisition range that is inversely proportional to the block size N. For example, if true CFO is $\omega_o = \pi$, then our CFO estimator
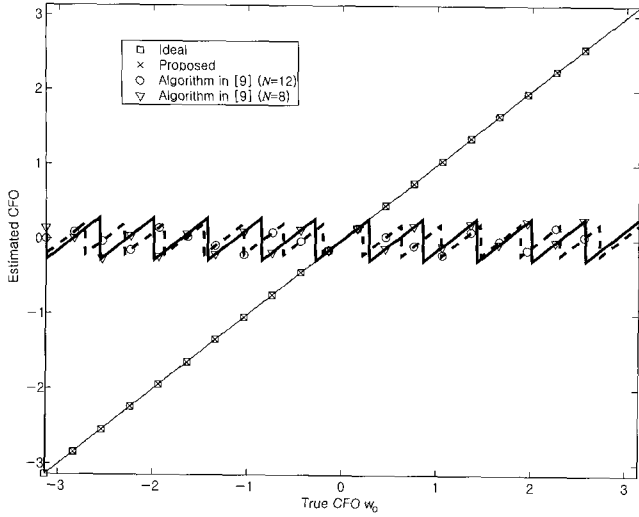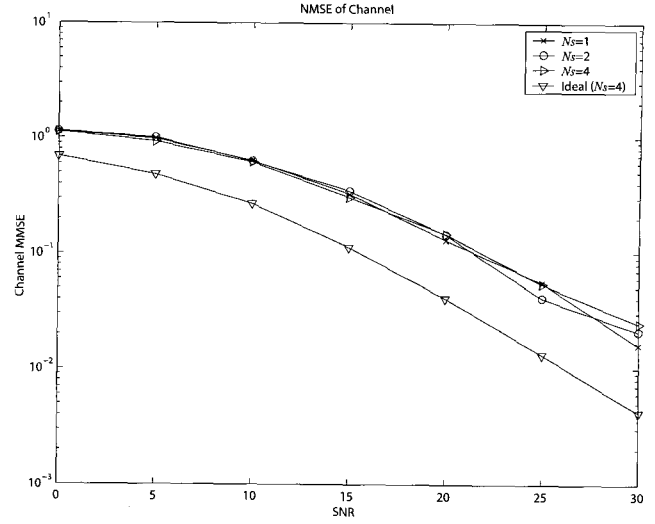
Fig. 3. CFO acquisition range comparison with channel order $L = 3$.

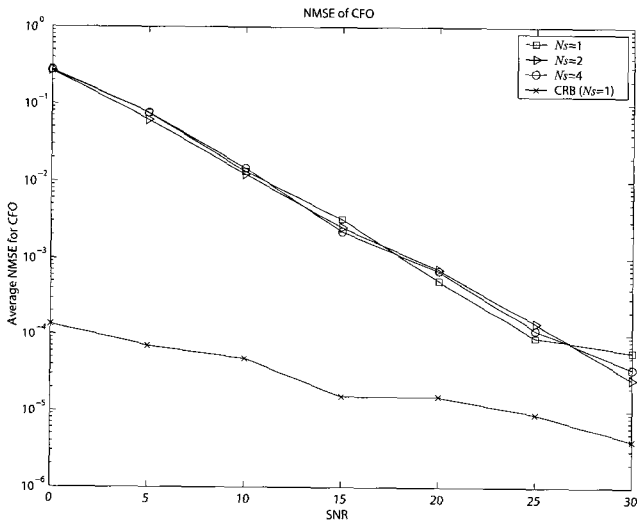

Fig. 5. Average normalized MSE for channels.

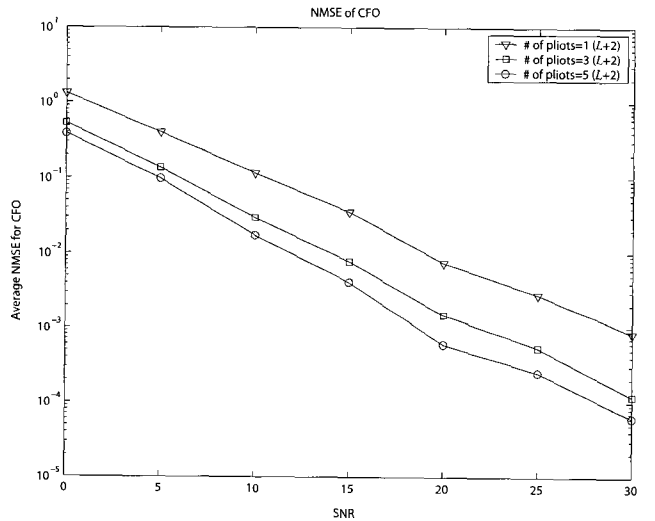Fig. 4. Average normalized MSE for CFO.

Fig. 6. Average normalized MSE of CFO for different number of pilots.

can give the estimated CFO, while [11] fails to estimate CFO, as shown in Fig. 3.

Example 2 (performance of CFO estimator): Fig. 4 shows average normalized mean square error (NMSE) of $\hat{\omega}_o$ for $N_s = 1, 2, 4$, where $L = 3$, and the CFOs are uniformly selected in the range $[-0.5\pi, 0.5\pi]$. The number of pilot symbols per node is $N_p = 4(L + 2)$, which is more than the minimum required number of pilot symbols $L + 2$. As a means of comparison, we calculated the normalized mean square error (NMSE) of CFO defined as $E[||\hat{\omega}_o - \omega_o||^2]/||\omega_o||^2$, where $\omega_o := [\omega_o^{(\nu,1)}, \cdots, \omega_o^{(\nu,N_s)}]^T$, and likewise for $\hat{\omega}_o$. The CRLB we derived in Section V is also shown as a benchmark. Thanks to the TDMA-based cooperative scheduling, we infer that the performance of our CFO estimators does not depend on the number of sensors.

Example 3 (performance of channel estimator): To test the performance of multi-channel estimation, we used $N_s = 1, 2, 4$, and $L = 3$, with the CFOs being randomly selected in the range of $[-0.5\pi, 0.5\pi]$. Single sensor CFO estimators

were calculated first as in (5). Based on the estimated CFOs, Fig. 5 shows channel estimation performance. To quantify channel estimation performance, we computed the average channel NMSE as $E[||\hat{h} - h||^2]/||h||^2$, where $\hat{h}$ was obtained using the LS method. The ideal case assuming perfect CFO estimation is shown for a benchmark to isolate the performance of channel estimation, which is also confirmed to be independent of the number of sensors.

Example 4 (tradeoff between performance and the number of pilots): Although the minimum number of pilots for our CFO and channel estimator is $L + 2$, the use of large number of pilots gives better performance, which will be demonstrated here. The parameters used in this example are the same with those in Examples 2 and 3. Since we already checked that the performance is independent of the number of sensors, we test the case of $N_s = 1$ with $N = 32$ and $L = 3$. Figs. 6 and 7 show the performance of CFO and channel estimator, respectively, when $N_p = 1(L+2)$, $3(L+2)$, and $5(L+2)$ are used. It is observed that our estimator with larger number of pilots achieves better
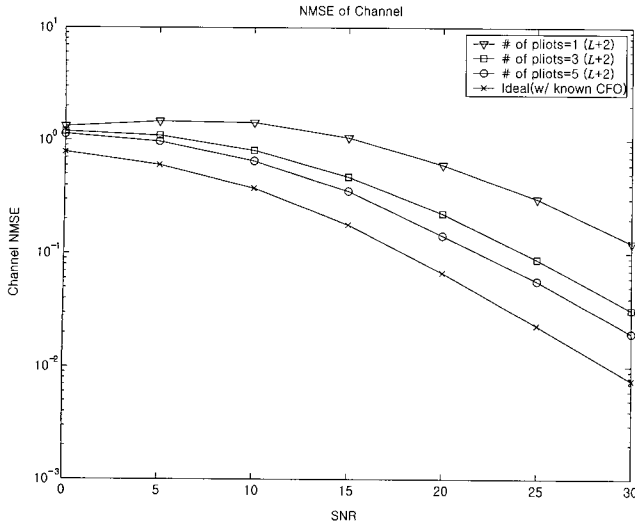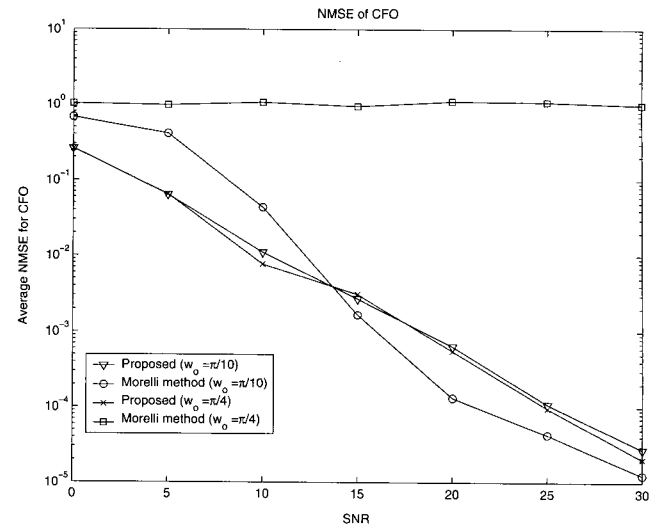
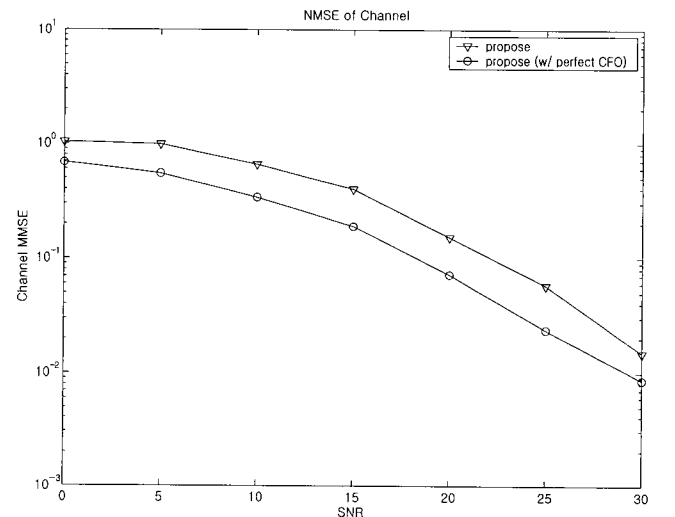Fig. 7. Average normalized channel MSE for different number of pilots.

Fig. 8. Average normalized CFO MSE for multi-carrier system ($N_s = 1$).

performance.

Example 5 (multi-carrier transmissions): To examine the performance of CFO and channel estimator with multi-carrier transmissions, we compare our method with an existing method in [17] for single antenna. For our algorithm, we use $N = 32$ (i.e., the number of subcarriers), carrier frequency 5 GHz, OFDM symbol (without CP) period 3.2 μs and signal bandwidth 10 MHz. To maintain the same transmission rate, the pilot length of [17] is 32 with 4 identical parts, i.e., the block length is also 32. In Fig. 8, two cases are considered: $\omega_o = \pi/10$ which is chosen within the acquisition range of the method in [17], and $\omega_o = \pi/4$ which is out of the acquisition range. If the CFO is chosen within the acquisition range of the method in [17], our method has comparable performance with the one in [17]. For the case of $\omega_o = \pi/4$, we also observe from Fig. 8 that our algorithm still enjoys performance comparable to the first case ($\omega_o = \pi/10$), while the method in [17] fails because its acquisition range is $\omega_o \in [-\pi/8, \pi/8]$. Moreover, different from the method in [17], our method also considers channel estimation. Fig. 9 shows the performance of the channel estimator. Although our channel estimator is not optimal for OFDM system, the proposed pilot design enables to estimate the CFO and channel together within one OFDM block.

VII. CONCLUSIONS

In this paper, we addressed synchronization and channel estimation in the context of wireless sensor networks. Based on judiciously designed pilot symbols, we separated CFO and channel estimation per node. The low complexity and low duty cycle features of our schemes make them attractive for power-limited sensor network operation. In addition to energy-efficiency, our CFO estimator exhibits full acquisition range. We also showed that our CFO and channel estimators can be used for multi-user multi-carrier systems. Both analytical and simulation results confirmed improved estimation performance relative to competing alternatives.

Fig. 9. Average normalized channel MSE for multi-carrier system ($N_s = 1$).

APPENDIX A: CRAMÉR-RAO LOWER BOUND

We derive Cramér-Rao lower bounds (CRLB) to benchmark our estimators. The input-output relationship for a single-sensor is given as $\mathbf{x} = \mathbf{D}_N(\omega_o)\mathbf{Hp} + \boldsymbol{\eta}$. Because convolution is a commutative operation, we deduce that $\mathbf{Hp} = \mathbf{Ph}$, where $\mathbf{P}$ is a Toeplitz matrix having elements $[\mathbf{P}]_{i,j} := p(i-j)$, $0 \le i \le N-1$, $0 \le j \le L$, which leads to $\mathbf{x} = \mathbf{D}_N(\omega_o)\mathbf{Ph} + \boldsymbol{\eta}$.

The CRLB for the CFO estimator is defined as

$$\text{CRLB}_{\omega_o} := \left(E\left[\left| \frac{\partial \ln p(\mathbf{x}|\omega_o, \mathbf{h})}{\partial \omega_o} \right|^2 \right] \right)^{-1} \tag{22}$$

where $p(\mathbf{x}|\omega_o, \mathbf{h})$ is the probability density function of $\mathbf{x}$ conditioned on ω_o and $\mathbf{h}$.

For a given $(\omega_o, \mathbf{h})$, the observation vector $\mathbf{x}$ is Gaussian with mean $\mathbf{D}_N(\omega_o)\mathbf{Ph}$, and covariance matrix $\sigma_\eta^2 \mathbf{I}_N$. Thus, the like-

lihood for the parameters $(\mathbf{h}, \omega_o)$ takes the form

$$p(\mathbf{x}|\omega_o, \mathbf{h}) =$$
$$\frac{1}{(2\pi\sigma_\eta^2)^N}\exp\left\{-\frac{1}{\sigma_\eta^2}[\mathbf{x} - \mathbf{D}_N(\omega_o)\mathbf{Ph}]^{\mathcal{H}}[\mathbf{x} - \mathbf{D}_N(\omega_o)\mathbf{Ph}]\right\}.$$

For one observation block, the log-likelihood function is given as

$$\ln p(\mathbf{x}|\omega_o, \mathbf{h}) =$$
$$N\ln(2\pi\sigma_\eta^2) - \frac{1}{\sigma_\eta^2}[\mathbf{x} - \mathbf{D}_N(\omega_o)\mathbf{Ph}]^{\mathcal{H}}[\mathbf{x} - \mathbf{D}_N(\omega_o)\mathbf{Ph}]. \quad (23)$$

By differentiating $\ln p(\mathbf{x}|\omega_o, \mathbf{h})$ as in (23) with respect to ω_o, we obtain that

$$\frac{\partial \ln p(\mathbf{x}|\omega_o, \mathbf{h})}{\partial \omega_o} = -\frac{2}{\sigma_\eta^2}\Im\left(\eta^{\mathcal{H}}\mathbf{D}(k)\mathbf{D}_N(\omega_o)\mathbf{Ph}\right) \quad (24)$$

where $\mathbf{D}(k) := \mathrm{diag}[0, 1, \cdots, N-1]$. Thus the Fisher information of CFO is given as

$$E\left[\left|\frac{\partial \ln p(\mathbf{x}|\omega_o, \mathbf{h})}{\partial \omega_o}\right|^2\right] = \frac{1}{\sigma_\eta^2}\mathrm{tr}\left[\mathbf{D}(k)\mathbf{PR}_h\mathbf{P}^{\mathcal{H}}\mathbf{D}(k)\right] \quad (25)$$

where $\mathbf{R}_h := E[\mathbf{hh}^{\mathcal{H}}]$. As a result, the CRLB of CFO estimator is given as the inverse of the Fisher information.

$$\mathrm{CRLB}_{\omega_o} = \left(\frac{1}{\sigma_\eta^2}\mathrm{tr}\left[\mathbf{D}(k)\mathbf{PR}_h\mathbf{P}^{\mathcal{H}}\mathbf{D}(k)\right]\right)^{-1} \quad (26)$$

APPENDIX B: PROOF OF (19) AND (20)

We derive an approximate closed form expression for the conditional mean and variance of $\hat{\omega}_o^{(\nu,\mu)}$ given $\omega_o^{(\nu,\mu)}$ and $\beta_{\nu,\mu}(n) := \sqrt{\mathcal{E}_p}\exp(j\omega_o^{(\nu,\mu)}n)\rho^n\sum_{l=0}^{L}h^{(\nu,\mu)}(l)\rho^{-l}$ for $n = (N_p+L)(\mu-1)+L, \cdots, (N_p+L)(\mu-1)+N_p-1$. To obtain the tangent of the phase error in (13), we have

$$\tan(\hat{\omega}_o^{(\nu,\mu)} - \omega_o^{(\nu,\mu)}) =$$
$$\left(\sum_{n=Q+L}^{Q+N_p-2}\Im[x_{\nu,\mu}(n+1)\rho^*x_{\nu,\mu}(n)^*e^{-j\omega_o^{(\nu,\mu)}}]\right)$$
$$/\left(\sum_{n=Q+L}^{Q+N_p-2}\Re[x_{\nu,\mu}(n+1)\rho^*x_{\nu,\mu}(n)^*e^{-j\omega_o^{(\nu,\mu)}}]\right) \quad (27)$$

where $Q := (N_p+L)(\mu-1)$. As $|\hat{\omega}_o^{(\nu,\mu)} - \omega_o^{(\nu,\mu)}| \ll 1$ holds for high SNR, the tangent can be approximated as

$$\hat{\omega}_o^{(\nu,\mu)} - \omega_o^{(\nu,\mu)} \simeq \left(\sum_{n=Q+L}^{Q+N_p-2}\Im[G]\right)/\left(\sum_{n=Q+L}^{Q+N_p-2}\Re[G]\right) \quad (28)$$

where $G := (\rho\beta_{\nu,\mu}(n) + \eta_\nu(n+1)e^{-j\omega_o^{(\nu,\mu)}})(\rho^*\beta_{\nu,\mu}^*(n) + \rho^*\eta_\nu^*(n))$. At high SNR, (28) can be approximated by

$$\hat{\omega}_o^{(\nu,\mu)} - \omega_o^{(\nu,\mu)} \simeq$$
$$\left(\sum_{n=Q+L}^{Q+N_p-2}\Im\left(\eta_\nu(n+1)\beta_{\nu,\mu}^*(n+1) + |\rho|^2\eta_\nu^*(n)\beta_{\nu,\mu}(n)\right)\right)$$
$$/\left(\sum_{n=Q+L}^{Q+N_p-2}|\rho|^2|\beta_{\nu,\mu}(n)|^2\right) \quad (29)$$

from which we can find that

$$E[\hat{\omega}_o^{(\nu,\mu)} - \omega_o^{(\nu,\mu)} \mid \omega_o^{(\nu,\mu)}, \{\beta_{\nu,\mu}(n)\}_{n=Q+L}^{Q+N_p-1}] = 0. \quad (30)$$

The conditional variance of our estimate can be easily determined by taking expectation of the square of (29) to result in

$$\frac{1}{2}E\left[\left\{\sum_{n=Q+L}^{Q+N_p-2}\eta_\nu(n+1)\beta_{\nu,\mu}^*(n+1) + |\rho|^2\sum_{n=Q+L}^{Q+N_p-2}\eta_\nu^*(n)\beta_{\nu,\mu}(n)\right\}^2\right]$$
$$/|\rho|^4E\left[\left\{\sum_{n=Q+L}^{Q+N_p-2}|\beta_{\nu,\mu}(n)|^2\right\}^2\right]. \quad (31)$$

Notice that we designed training symbols so that $|\rho|^2 = 1$ and noise variance $\sigma_{\eta_\nu}^2 = N_o/2$. Thus we can obtain from (31) that

$$\frac{1}{4|\rho|^4}(1 + |\rho|^4)\frac{1}{\mathcal{E}_t/N_o} = \frac{1}{2}\frac{1}{\mathcal{E}_t/N_o} \quad (32)$$

where $\mathcal{E}_t$ is the received total signal energy for an interval where CFO estimation can be performed, which is defined as

$$\mathcal{E}_t = \sum_{n=Q+L}^{Q+N_p-2} E\left[\beta_{\nu,\mu}(n)\beta_{\nu,\mu}^*(n)\right]$$
$$= (N_p - L - 1)\mathcal{E}_p\sum_{l=0}^{L}|h^{(\nu,\mu)}(l)|^2. \quad (33)$$

Finally, we have

$$\mathrm{Var}[\hat{\omega}_o^{(\nu,\mu)} \mid \omega_o^{(\nu,\mu)}, \{\beta_{\nu,\mu}(n)\}_{n=Q+L}^{Q+N_p-1}] = \frac{1}{(N_p - L - 1)\mathrm{SNR}} \quad (34)$$

where $\mathrm{SNR} := (\mathcal{E}_p/\sigma_{\eta_\nu}^2)\sum_{l=0}^{L}|h^{(\nu,\mu)}(l)|^2$.

APPENDIX C: DERIVATION OF (16) FROM (15)

Let us consider a vector $\mathbf{u}_\mu := [u_\mu(0), \cdots, u_\mu(N-1)]^T$ with length N, for the μ-th mobile user. In OFDM system, we implement N-point inverse FFT (via left multiplication with $\mathbf{F}_N^{\mathcal{H}}$) on each block $\mathbf{u}_\mu$ and insert the cyclic prefix (via left multiplication with the matrix operator $\mathbf{T}_{cp} := [\mathbf{I}_{L\times N}^T\ \mathbf{I}_N^T]^T$, where $\mathbf{I}_{L\times N}$ denotes the last L columns of $\mathbf{I}_N$). After parallel to serial (P/S) conversion, the resulting blocks $\{\tilde{\mathbf{u}}_\mu := \mathbf{T}_{cp}\mathbf{F}_N^T\mathbf{u}_\mu\}$

of size $P \times 1$ are transmitted through frequency selective channel, where $P = N + L$.

The received samples at the ν-th antenna in the base station are given by (15). The sequence $x_\nu(n)$ is then serial to parallel (S/P) converted into $P \times 1$ blocks with entries $x_\nu := [x_\nu(0), \cdots, x_\nu(P-1)]^T$. Then, we discard the cyclic prefix of length L by left multiplying x_ν with the matrix $R_{cp} := [0_{N \times L} \ I_N]$. Denoting the resulting block as $y_\nu := R_{cp}x_\nu$, we obtain the following vector-matrix input-output relationship.

$$y_\nu = \sum_{\mu=1}^{N_s} R_{cp}D_P(\omega_o^{(\nu,\mu)})H^{(\nu,\mu)}T_{cp}F_N^{\mathcal{H}}u_\mu + R_{cp}\eta_\nu \quad (35)$$

$\nu \in [1, N_s]$, where $\eta_\nu := [\eta_\nu(0), \eta_\nu(1), \cdots, \eta_\nu(P-1)]^T$, with $P = N + L$; $H^{(\nu,\mu)}$ is a $P \times P$ lower triangular Toeplitz matrix with first column $[h^{(\nu,\mu)}(0), \cdots, h^{(\nu,\mu)}(L), 0, \cdots, 0]^T$; and $D_P(\omega_o^{(\nu,\mu)})$ is a diagonal matrix defined as $D_P(\omega_o^{(\nu,\mu)}) := \text{diag}[1, e^{j\omega_o^{(\nu,\mu)}}, \cdots, e^{j\omega_o^{(\nu,\mu)}(P-1)}]$.

Based on the structure of the matrices involved, it can be readily verified that $R_{cp}D_P(\omega_o^{(\nu,\mu)}) = e^{j\omega_o^{(\nu,\mu)}L}D_N(\omega_o^{(\nu,\mu)})R_{cp}$, where $D_N(\omega_o^{(\nu,\mu)}) := \text{diag}[1, e^{j\omega_o^{(\nu,\mu)}}, \cdots, e^{j\omega_o^{(\nu,\mu)}(N-1)}]$. Following this identity, let us define $\tilde{H}^{(\nu,\mu)} := R_{cp}H^{(\nu,\mu)}T_{cp}$, where the $N \times N$ matrix $\tilde{H}^{(\nu,\mu)}$ is circulant with first column $[h^{(\nu,\mu)}(0), \cdots, h^{(\nu,\mu)}(L), 0, \cdots, 0]^T$. Letting also $v_\nu := R_{cp}\eta_\nu$, we can rewrite (35) as

$$y_\nu = \sum_{\mu=1}^{N_s} e^{j\omega_o^{(\nu,\mu)}L}D_N(\omega_o^{(\nu,\mu)})\tilde{H}^{(\nu,\mu)}F_N^{\mathcal{H}}u_\mu + v_\nu \quad (36)$$

which turns out to be (16).

In the absence of CFO ($\omega_o^{(\nu,\mu)} = 0$), taking the FFT of y_ν gives the frequency selective channel equivalent to a set of flat-fading subchannels, i.e., the conventional MIMO-OFDM system [16]

$$\bar{y} := F_N y_\nu = \sum_{\mu=1}^{N_s} D_N(\tilde{h}^{(\nu,\mu)})u_\mu + F_N u_\nu \quad (37)$$

where we use the fact that $F_N \tilde{H}^{(\nu,\mu)} F_N^{\mathcal{H}}$ is a diagonal matrix $D_N(\tilde{h}^{(\nu,\mu)})$, for which $\tilde{h}^{(\nu,\mu)} := [\tilde{h}^{(\nu,\mu)}(0), \cdots, \tilde{h}^{(\nu,\mu)}(2\pi(N-1)/N)]^T$ with $\tilde{h}^{(\nu,\mu)}(2\pi n/N)$ denoting the (ν, μ)-th channel's frequency response value on the n-th FFT grid, which is given by $\tilde{h}^{(\nu,\mu)}(2\pi n/N) := \sum_{l=0}^L h^{(\nu,\mu)}(l) \exp(-j2\pi ln/N)$.

ACKNOWLEDGEMENT

REFERENCES

[1] I. F. Akyildiz, W. Su, Y. Sankarasubramaniam, and E. Cayirci, "A survey on sensor networks," *IEEE Commun. Mag.*, vol. 40, pp. 102–114, Aug. 2002.

[2] D. N. Jayasimha, S. S. Iyengar, and R. L. Kashyap, "Information integration and synchronization in distributed sensor networks," *IEEE Trans. Syst., Man, Cybern.*, vol. 21, pp. 1032–1043, Sept./Oct. 1991.

[3] E. H. Callaway, *Wireless Sensor Networks-Architectures and Protocols*, Auerbach, 2004.

[4] J. N. Laneman and G. W. Wornell, "Distributed space-time coded protocols for exploiting cooperative diversity in wireless networks," *IEEE Trans. Inform. Theory*, vol. 49, pp. 2415–2425, Oct. 2003.

[5] G. J. Foschini and M. J. Gans, "On limits of wireless communication in a fading environment when using multiple antennas," *Wireless Pers. Commun.*, vol. 6, no. 3, pp. 311–335, Mar. 1998.

[6] G. J. Foschini, "Layered space-time architecture for wireless communication in a fading environment when using multi-element antenna," *Bell Labs. Tech. J.*, vol. 1, pp. 41–59, 1996.

[7] V. Tarokh, H. Jafarkhami, and A. R. Calderbank, "Space-time block codes from orthogonal designs," *IEEE Trans. Inform. Theory*, vol. 45, pp. 1456–1467, July 1999.

[8] X. Ma, L. Yang, and G. B. Giannakis, "Optimal training for MIMO frequency-selective fading channels," *IEEE Trans. Wireless Commun.*, vol. 4, pp. 453–466, Mar. 2005.

[9] R. Negi and J. Cioffi, "Pilot tone selection for channel estimation in a mobile OFDM system," *IEEE Trans. Consumer Electron.*, vol. 44, no. 3, pp. 1122–1128, Aug. 1998.

[10] Q. Sun, D. C. Cox, and H. C. Huang, "Estimation of continuous flat fading MIMO channel," *IEEE Trans. Wireless Commun.*, vol. 1, no. 4, pp. 549–553, Oct. 2002.

[11] P. H. Moose, "A technique for orthogonal frequency division multiplexing frequency offset correction," *IEEE Trans. Commun.*, vol. 42, pp. 2908–1314, Oct. 1994.

[12] M. Morelli and U. Mengali, "Carrier-frequency estimation for transmissions over selective channels," *IEEE Trans. Commun.*, vol. 48, no. 9, pp. 1580–1589, Sep. 2000.

[13] X. Ma, C. Tepedelenlioglu, G. B. Giannakis, and S. Barbarossa, "Non-data-aided carrier offset estimation for OFDM with null subcarriers: Identifiability, algorithms, and performance," *IEEE Trans. Commun.*, vol. 19, no. 12, pp. 2504–2515, Dec. 2001.

[14] Y. D. Kim, J. K. Lim, C. H. Shu, E. R. Jung, and Y. H. Lee, "Carrier frequency estimation for transmissions with antenna diversity," in *Proc. VTC 2002*, vol. 3, 2002, pp. 1569–1573.

[15] J. Kivinen, T. O. Korhonen, P. Aikio, R. Gruber, P. Vainikainen, and S. G. Haggman, "Wideband radio channel measurement system at 2 GHz," *IEEE Trans. Instrum. Meas.*, vol. 48, issue 1, pp. 39–44, Feb. 1999.

[16] X. Ma, M.-K. Oh, G. B. Giannakis, and D.-J. Park, "Hopping pilots for estimation of frequency-offset and multiantenna channels in MIMO-OFDM," *IEEE Trans. Commun.*, vol. 53, no. 1, pp. 162–172, Jan. 2005.

[17] M. Morelli and U. Mengali, "An improved frequency offset estimator for OFDM applicatins," *IEEE Commun. Lett.*, vol. 3, no. 3, pp. 75–77, Mar. 1999.

[18] G. H. Golub and C. F. van Loan, *Matrix Computations*, 3rd ed., Baltimore, MD: Johns Hopkins Univ. Press, 1996.

[19] J. G. Proakis, *Digital Communications*, 4-th ed., McGraw-Hill, 2000.

[20] M. L. Sichitiu and C. Veerarittiphan, "Simple, accurate time synchronization for wireless sensor networks," in *Proc. IEEE WCNC 2003*, vol. 2, Mar. 2003, pp. 1266–1273.

[21] Z. Wang and G. B. Giannakis, "Wireless multicarrier communications: Where Fourier meets Shannon," *IEEE Signal Processing Mag.*, vol. 47, pp. 29–48, May 2000.

[22] K. Yao, R. E. Hudson, C. W. Reed, and D. Chen, "Blind beamforming on a randomly distributed sensor array system," *IEEE J. Select. Areas Commun.*, vol. 16, pp. 1555–1567, Oct. 1998.

[23] T. Pollet, M. Van Bladel, and M. Moenecley, "BER sensitivity of OFDM systems to carrier frequency offset and Wiener phase noise," *IEEE Trans. Commun.*, vol. 43, no. 234, pp. 191–193, Feb./Mar./Apr. 1995.

Mi-Kyung Oh received the B.S. degree from the Department of Electrical Engineering, Chung-ang University, Korea in 2000 and the M.S. degree in Electrical Engineering from the Korea Advanced Institute of Science and Technology (KAIST), Korea in 2002. From September 2002 to February 2004, she was a visiting researcher in the Department of Electrical and Computer Engineering at the University of Minnesota. She is currently the Ph.D. candidate of the Department of Electrical Engineering and Computer Science in KAIST. Her research interests include channel estimation, synchronization, wireless networks, and channel coding.
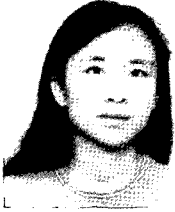
Xiaoli Ma received the B.S. degree in automatic control from Tsinghua University, Beijing, P.R. China, in 1998 and the M.Sc. and Ph.D. degrees in electrical engineering from the University of Virginia, Charlottesville, VA, in 1999 and the University of Minnesota, Minneapolis, MN, in 2003, respectively. Since Aug. 2003, she has been an assistant professor with the Department of Electrical and Computer Engineering, Auburn University. Her research interests include transmitter and receiver diversity techniques for wireless fading channels, communications over time and frequency selective channels, complex-field and space-time coding, channel estimation and equalization algorithms, carrier frequency synchronization for OFDM systems, and wireless sensor networks.

Dong-Jo Park received the B.S. degree from the Department of Electrical Engineering, Seoul National University, Korea in 1976 and the M.S. and Ph.D. degrees in Electrical Engineering from the University of California, Los Angeles, U.S.A. in 1981 and 1984, respectively. He was a senior researcher of Electronics and Telecommunications Research Institute (ETRI), Daejeon, Korea, from 1984 to 1985. He is currently professor in the Department of Electronic and Computer Science in Korea Advanced Institute of Science and Technology (KAIST), Daejeon, Korea. His research interests include multi-input multi-output systems, OFDM, multi-media signal processing, ultra-wide band communications, and channel coding. He is a member of IEEE, IEICE, KIEE, KICS, and KISS.
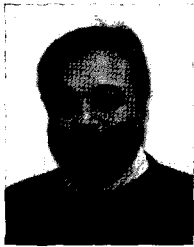
Georgios. B. Giannakis received his Diploma in Electrical Engineering from the National Technical University of Athens, Greece, 1981. From September 1982 to July 1986, he was with the University of Southern California (USC), where he received his M.Sc. in Electrical Engineering, 1983, M.Sc. in Mathematics, 1986, and Ph.D. in Electrical Engineering, 1986. After lecturing for one year at USC, he joined the University of Virginia in 1987, where he became a professor of Electrical Engineering in 1997. Since 1999, he has been a professor with the Department of Electrical and Computer Engineering at the University of Minnesota, where he now holds an ADC Chair in Wireless Telecommunications.

His general interests span the areas of communications and signal processing, estimation and detection theory, time-series analysis, and system identification—subjects on which he has published more than 200 journal papers, 350 conference papers, and two edited books. Current research focuses on transmitter and receiver diversity techniques for single- and multi-user fading communication channels, complex-field and space-time coding, multicarrier, ultra-wide band wireless communication systems, cross-layer designs, and sensor networks.

G. B. Giannakis is the (co-) recipient of six paper awards from the IEEE Signal Processing (SP) and Communications Societies (1992, 1998, 2000, 2001, 2003, and 2004). He also received the SP Society's Technical Achievement Award in 2000. He served as Editor in Chief for the *IEEE SP Letters*, as Associate Editor for the *IEEE Trans. Signal Proc.* and the *IEEE SP Letters*, as secretary of the SP Conference Board, as member of the SP Publications Board, as member and vice-chair of the Statistical Signal and Array Processing Technical Committee, as chair of the SP for Communications Technical Committee and as a member of the IEEE Fellows Election Committee. He has also served as a member of the IEEE-SP Society's Board of Governors, the Editorial Board for the *Proceedings of the IEEE* and the steering committee of the *IEEE Trans. Wireless Commun.*.